Chemical Science

ROYAL SOCIETY OF CHEMISTRY

EDGE ARTICLE

View Article Online
View Journal | View Issue

Cite this: *Chem. Sci.*, 2025, **16**, 15597

All publication charges for this article have been paid for by the Royal Society of Chemistry

Received 27th March 2025
Accepted 19th July 2025

DOI: 10.1039/d5sc02348c

rsc.li/chemical-science

Air-processed, ultraresponsive NIR photodetectors using 2D perovskite hybrids†

Dulce Zugasti-Fernández, [a] Priscila I. Román-Román, [a] Mara Gutierrez-Avila,[a] A. Paulina Gómora-Figueroa,[b] Juan Hernández-Cordero, [a] Vojtech Jancik,[cd] Norberto Hernández-Como[e] and Diego Solis-Ibarra *[a]

Halide perovskites have shown tremendous potential as active materials in various optoelectronic devices, including solar cells, light-emitting diodes and photodetectors. However, their relatively large bandgaps – typically limited to ~1.40 eV (~885 nm) – constrain their use as near-infrared (NIR) photodetectors. Here, we present a novel two-dimensional (2D) hybrid perovskite $(PDA)_2PbI_4$ (PDA = 6-phenyl-3,5-hexadiynylammonium), which upon thermopolymerization forms (poly-PDA) PbI_4 (polyPDA = polymerized PDA). This material can be incorporated into NIR photodetectors exhibiting record-high responsivities of up to 10^7 A W^{-1} and external quantum efficiencies of up to (128.0 ± 3.6)% at 980 nm under a 4 V bias. Notably, the devices can be fabricated, operated, and stored entirely under ambient air conditions, highlighting their stability and processability.

Introduction

Metal halide perovskites (MHPs) are promising candidates for multiple applications such as solar cells,[1] light-emitting diodes,[2] phosphors and various other optoelectronic applications.[3] Among these, photodetectors – devices that detect and quantify incident radiation – have garnered increasing interest due to their broad applicability in communications,[4] security, imaging, and sensing technology.[5] To date, MHPs and MHPs-inspired materials have shown great promise for photodetection in several regions of the spectrum, including ionizing radiation, X-ray, UV and visible light.[6–8] Nevertheless, there have been relatively few reports on near-infrared (NIR) detection, primarily because MHPs exhibit limited absorption in this spectral region due to their relatively large bandgaps (~1.40 eV, ~885 nm, at best).[9] Furthermore, the few perovskite-based devices capable of detecting NIR radiation typically rely on tin or tin-lead perovskites, which significantly limit air processability and stability.[10]

Previously, it has been shown that the incorporation of molecules with two adjacent C≡C triple bonds, also known as dyines, into a layered perovskite and their subsequent polymerization by means of thermal treatment allows for the improvement of conductivity generating free carriers, and most importantly, extending the absorption edge of materials well into the NIR region of the spectrum.[11,12] Motivated by this, we decided to explore this approach to fabricate NIR-photodetectors, which, as discussed earlier, are traditionally inaccessible to MHPs and MHPs-inspired materials.

Herein, we report on a novel material: $(PDA)_2PbI_4$ (PDA = 6-phenyl-3,5-hexadiynylammonium), which upon thermopolymerization forms $(poly\text{-}PDA)_2PbI_4$ (poly-PDA = polymerized PDA), can be used as active material in ultraresponsive NIR-photodetectors. These devices achieve remarkable responsivities of up to 10^7 A W^{-1} and external quantum efficiencies (EQE) of up to 128.0 ± 3.6% at 980 nm. Furthermore, they exhibit responsivities comparable to state-of-the-art devices,[13,14] while being fully air-processable and maintaining stability for up to two months in ambient conditions.

Results and discussion

First, we synthesized 6-phenyl-3,5-hexadiynylamine in a two-step synthesis with an overall yield of 64% (see ESI† for full synthetic procedure). To synthesize $(PDA)_2PbI_4$, the free amine is dissolved in ethanol and mixed with a solution of PbI_2 and HI. From this mixture, $(PDA)_2PbI_4$ crystallizes as yellowish plate-like crystals, which were first characterized using single-

[a]*Instituto de Investigaciones en Materiales, Universidad Nacional Autónoma de México, Ciudad Universitaria, A.P. 70-360, Coyoacán, Mexico City, 04510, Mexico. E-mail: diego.solis@unam.mx*

[b]*Facultad de Ingeniería, Universidad Nacional Autónoma de México (UNAM), Coyoacán, Ciudad de México, 04510, Mexico*

[c]*Instituto de Química, Universidad Nacional Autónoma de México, Ciudad Universitaria, 04510, Mexico*

[d]*Centro Conjunto de Investigación en Química Sustentable UAEM-UNAM, Carretera Toluca Atlacomulco km. 14.5, Toluca, Estado de México, Mexico*

[e]*Centro de Nanociencias y Micro y Nanotecnologías, Instituto Politécnico Nacional, Unidad Profesional Adolfo López Mateos, Av. Luis Enrique Erro S/N, Zacatenco, Alcaldía Gustavo A. Madero, CP 07738, Mexico*

† Electronic supplementary information (ESI) available. CCDC 2432056. For ESI and crystallographic data in CIF or other electronic format see DOI: https://doi.org/10.1039/d5sc02348c

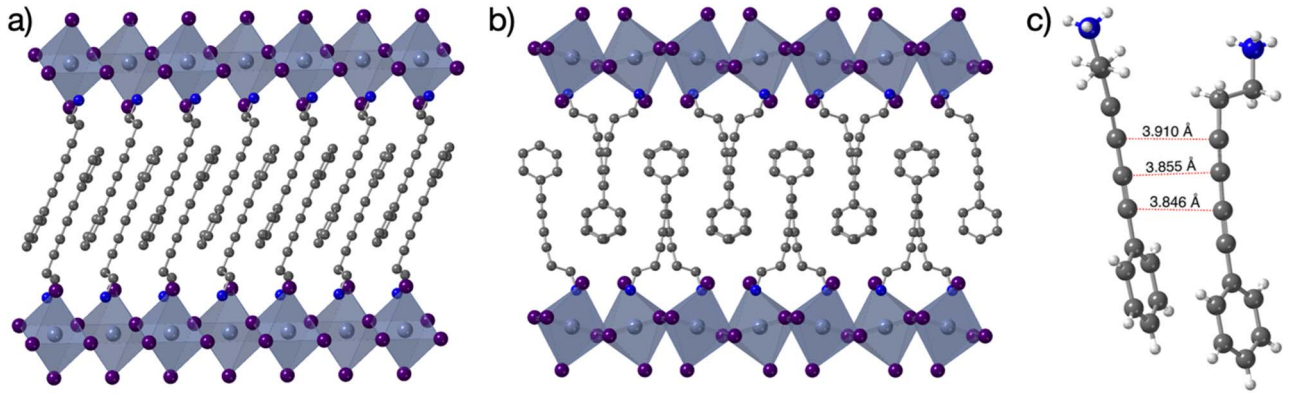

Fig. 1 (a) and (b) Crystal structure of $(PDA)_2PbI_4$ seen from b and c, respectively (a and b). Hydrogen-bonds were omitted for clarity. Purple: iodine, light blue: lead, dark blue: nitrogen, grey: carbon. (c) Selected Csp···Csp distances found within the structure of $(PDA)_2PbI_4$, dark blue: nitrogen, grey: carbon, white: hydrogen.

crystal X-ray diffraction (SC-XRD) and powder X-ray diffraction (PXRD).

These characterization techniques confirmed the formation of a two-dimensional (2D) perovskite that incorporates PDA in between the layers (Fig. 1a and b) and the phase purity of the obtained solid (Fig. 2). Similarly, from the single crystal X-ray structure, it can be observed that triple bonds remain such, with the expected short C≡C distances of 1.193 and 1.206 Å and nearly 177.14 and 177.25°. From the single-crystal X-ray structure it is also notable that the PDA ligands show significant interdigitation and short Csp···Csp of 3.91, 3.86 and 3.85 Å (Fig. 1c), suggesting that a post synthetic polymerization is feasible. We then looked for possible polymerization events using differential scanning calorimetry (DSC), showing an endothermic event at 180 °C, which prompted us to try thermal treatment at this temperature (Fig. S16†).

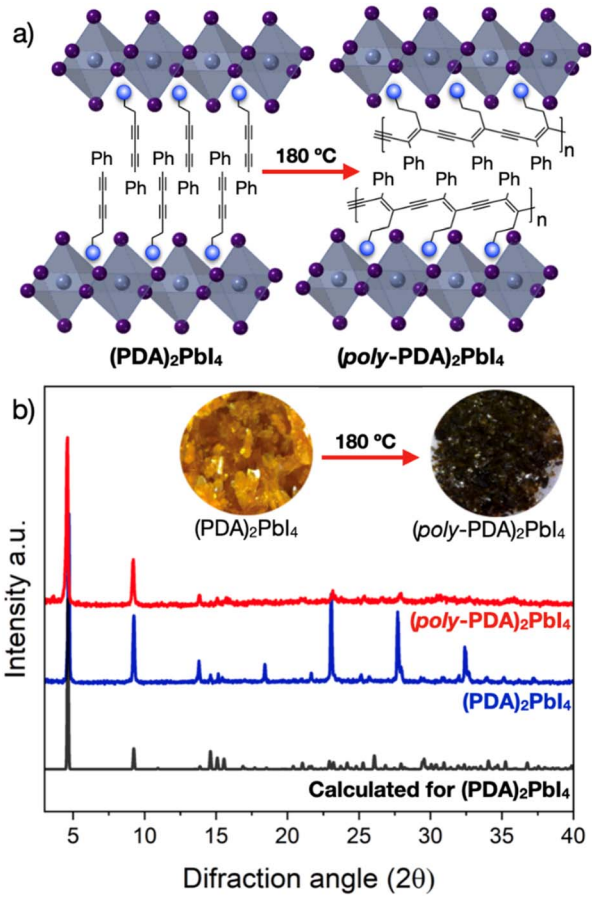

Fig. 2 (a) Schematic representation of the polymerization process of $(PDA)_2PbI_4$ to form $(poly\text{-}PDA)_2PbI_4$. (b) Powder X-ray diffraction of $(PDA)_2PbI_4$ (blue line), $(poly\text{-}PDA)_2PbI_4$ (red line) and the calculated PXRD pattern of $(PDA)_2PbI_4$ crystal structure. Inset: photographs of $(poly\text{-}PDA)_2PbI_4$ and $(poly\text{-}PDA)_2PbI_4$.

After four hours of treatment, a drastic colour change was observed resulting in a black crystalline solid, from here on referred to as $(poly\text{-}PDA)_2PbI_4$. Notably, $(poly\text{-}PDA)_2PbI_4$ maintains its crystallinity, as seen from its physical appearance, and from its powder X-ray diffraction (PXRD) (Fig. 2). Further, a slight elongation of the *c*-axis of about 0.5 Å is observed, as evidenced by a shift in the <*n*00> diffraction planes towards smaller angles. The small shift in those planes is also consistent with a polymerization process.

To analyse the nature of the organic fragment and corroborate that the polymerization occurs upon thermal treatment, we performed a ^{13}C Attached Proton Test (APT) Nuclear Magnetic Resonance (NMR) spectroscopy. We found seven additional signals that are absent in the starting ligand's spectrum prior to thermal treatment, supporting the hypothesis that the thermal treatment generates structural modifications on the organic part of the material (Fig. S13†). The signals observed at δ 131.9–131.7 ppm, δ 129.0–128.8 ppm, δ 126.7 ppm, and δ 103.4 ppm correspond to C–H carbons, and the singlet at 38.6 ppm could be related to a new quaternary carbon or CH_2, indicating the formation of new sp^3 hybridized bond. The emergence of these signals is consistent with the polymerization reaction within the crystal structure. Then, NMR (^1H) analysis was performed to determine the polymerization yield, using quantitative with 1,2,4,5-tetrachloro-3-nitrobenzene as standard (TCNB) obtaining 83% yield of the polymerized organic fragment (Fig. S14†).

To evaluate the effect of heat treatment on the optical absorption of the material, we performed UV-Vis-NIR spectroscopy analysis before and after the treatment (Fig. S9†). Before

treatment, the absorption spectra of $(PDA)_2PbI_4$ showed the characteristic absorption features of a lead-iodide 2D hybrid perovskite, with an estimated bandgap of 2.3 eV (Fig. S10†). After treatment the material had a black colour and the absorption spectrum covered a much wider range of wavelengths, from UV to near infrared, with a bandgap of 1.2 eV (Fig. S11†).

Motivated by its absorption, we decided to test (poly-PDA)$_2$-PbI_4 as an active photodetector material. Devices were fabricated using interdigitated gold electrodes (100 nm thick) deposited on glass substrates *via* photolithography (Fig. 3a and b). The fabrication process was optimized to enable polymerization of $(PDA)_2PbI_4$ directly on the substrate, while maintaining the crystallinity and integrity of the material and the films, which are critical for device performance. Films were deposited *via* drop-casting and gradually heated from 25 to 110 °C, a significantly lower temperature than the required for the bulk material (180 °C),[15] as supported by UV-Vis-NIR analysis (see ESI S18†).

To verify the photodetectors' functionality and determine their sensitivity to infrared light, a 980 nm laser diode was used to irradiate them. The dark current of the devices was measured to determine its response to different light intensities (Fig. 3c and Table S4†) and at different bias voltages (Fig. S19–S22†). A comparison among devices with various electrode separations revealed an optimal distance of 100 μm, which provided the highest responsivity and EQE values under fixed illumination and bias. The trends observed suggest a balance between charge collection efficiency and carrier recombination.[16]

A complete analysis of the performance metrics and the electrodes configuration are presented in the ESI.† We note that the best responsivity for devices made with (poly-PDA)$_2PbI_4$ as the active material ($1.76 \pm 0.048 \times 10^7$ A W^{-1}, average for four devices), is comparable with state-of-the-art perovskite devices, such as those based on single-crystalline thin-film of $MAPbBr_3$ (1.6×10^{-7} A W^{-1}),[13] field-effect phototransistors based on $CsPbBr_3$–PbS colloidal quantum dots heterostructure (4.5×10^5 A W^{-1})[17] or nanowire arrays of $MAPb(I_{1-x}Br_x)_3$ (1.2×10^4 A W^{-1}),[18] all of which detect at 780 nm or below. Also, its responsivity is comparable with some of the best reported NIR photodetectors, such as Si/SiO_2/hybrid graphene-PbS quantum dots devices ($\sim 5 \times 10^7$ A W^{-1}),[19] a double barrier structure of $In_{0.53}Ga_{0.47}As$ (4.19×10^5 A W^{-1}),[20] or BODIPY-BF2-based phototransistors (1.14×10^4 A W^{-1}).[21] From this analysis, it should be noted that the EQE at 980 nm reaches up to $128.0 \pm 3.6\%$, while the dark current was estimated to be $1.06 \pm 0.019 \times 10^{-6}$ A at 4 V bias, which is not optimal, but expected, given the device architecture.[22] Subsequently, we evaluated the temporal response of the devices (Fig. 3d). From the collected data, we calculated the response time under a 4 V bias. The rise time—defined as the time required for the signal to increase from 10% to 90% of its saturation value—was 6.73 s, while the fall time—corresponding to the signal's decrease from 90% to 10%—was 2.74 s (Fig. S25†). These values, although modest, are consistent with expectations given the device architecture and the polycrystalline nature of the films. In future work, scalable deposition techniques such as ultrasonic spray synthesis could be explored to improve the film uniformity and crystal orientation, thereby enhancing optoelectronic performance.[6]

Unfortunately, we were unable to polymerize PDA on its own to fabricate control devices using poly-PDA in the absence of the perovskite matrix. Such a comparison would have allowed us to evaluate the individual contributions of the organic and inorganic components, specifically to assess whether the perovskite framework offers advantages beyond those of the polymer alone. Nevertheless, it is worth noting that, to the best of our knowledge, there are very few reports of photodetectors based solely on polyacetylenes as the active material—that is, devices where polyacetylene is not used as part of a blend or composite. This scarcity is likely due to the intrinsically low carrier mobilities of these polymers.[23] While further studies are needed, we hypothesize that the perovskite framework enables a more controlled and oriented polymerization, which not only enhances processability but also improves carrier mobility, thereby making the resulting material suitable for photodetector applications.

To evaluate the impact of different π-functionalized organic cations, we prepared analogous devices using the previously reported (poly-DDA)$_2PbI_4$, where DDA = 3,5-decadiynediammonium (see ESI† for details), as the active material.[11,12] Like PDA, DDA contains two conjugated alkyne moieties along its carbon backbone, offering partial π-delocalization and structural rigidity. However, DDA contains a terminal *n*-butyl fragment instead of the phenyl ring in PDA, thus reducing its electronic delocalization and increasing the steric repulsion between the organic layers in the hybrid perovskite framework. Photoresponse measurements were performed under the same conditions as for (poly-PDA)$_2PbI_4$ devices. Notably, devices made of (poly-DDA)$_2PbI_4$, showed a significantly lower detection limit, preventing us from comparing both photodetectors at low light intensities – where (poly-PDA)$_2PbI_4$ performs the best. Hence, for a direct comparison, we evaluated its responsivity under an incident light of 980 nm at a power of 15 mW. At this power, (poly-PDA)$_2PbI_4$ based photodetectors exhibited a responsivity of 30.9 ± 0.5 A W^{-1}, whereas (poly-DDA)$_2PbI_4$ showed 1.2 ± 0.1 A W^{-1}, a decrease of over one order in magnitude. Fig. S31† presents a comparison of responsivity values for both devices across a range of light intensities. Devices based on (poly-PDA)$_2PbI_4$ consistently outperformed those based on (poly-DDA)$_2PbI_4$, particularly under weak illumination. This trend suggests that enhanced photoconductive gain in (poly-PDA)$_2PbI_4$-based devices, can be attributed to the shorter molecular structure of PDA, promoting tighter interlayer packing, shorter π–π interactions, and increased dielectric screening. These factors collectively facilitate more efficient charge transport. In contrast, the bulkier aliphatic chain in DDA impedes charge mobility, resulting in reduced photo-response.

The high responsivity and EQE values obtained for (poly-PDA)$_2PbI_4$-based devices confirm the exceptional potential of this material, likely enhanced by extended π-conjugation provided by both the diynyl chain and the terminal aromatic ring. Interestingly, the (poly-DDA)$_2PbI_4$-based devices also exhibit a non-negligible photoresponse, despite the absence of an aromatic moiety. This result supports the idea that partial π-conjugation – introduced by conjugated alkynes plays a significant role in enhancing charge transport and photogeneration

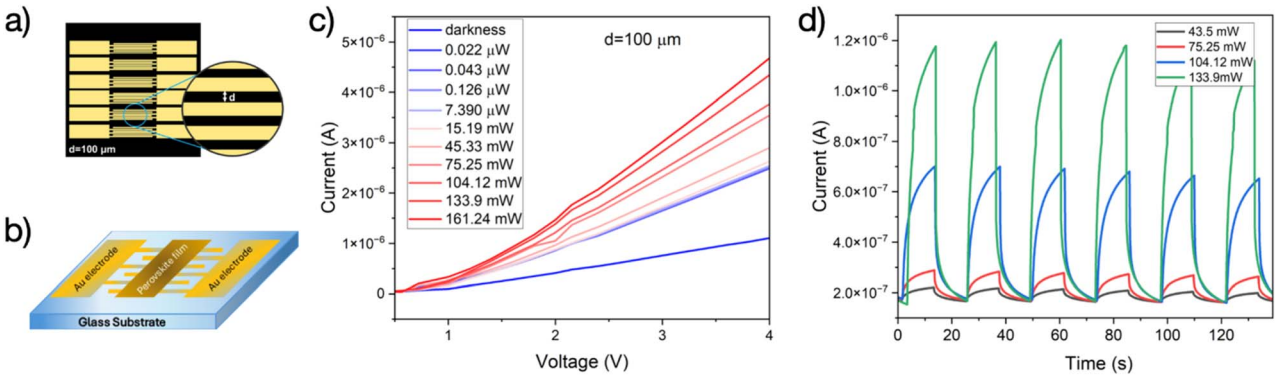

Fig. 3 (a) Interdigitated electrode architecture and (b) and schematic device architecture (c). Current–voltage (*I*–*V*) characteristics of the photodetector at varying bias voltages and laser optical powers (at 980 nm) for an interelectrode spacing of 100 μm. (d) Temporal photoresponse of the photodetector under a 4 V bias voltage at different optical power levels (also at 980 nm).

efficiency. Thus, the comparative analysis between both materials reveals a structure–function correlation and suggests that further improvements could be achieved through molecular engineering of the organic spacer.

Finally, we evaluated the stability of the devices, noting that all material synthesis and device fabrication were performed under ambient conditions, without the need for inert atmospheres or anhydrous solvents. Similarly, the devices were stored on a standard, non-dried shelf and tested after two months. Remarkably, even after this period, they retained 84% of their original performance (Fig. S25†). Since PXRD analysis showed no signs of material decomposition, we attribute this performance decline primarily to degradation at the interface between the gold electrodes and the material.

Conclusions

We have demonstrated that the novel perovskite (poly-PDA)$_2$-PbI$_4$ is an effective active material for NIR photodetectors. Owing to its unique properties, our devices exhibit an extended detection range that surpasses most, if not all, MHP-based photodetectors, while achieving ultrahigh responsivity. Notably, the devices can be fully assembled under ambient conditions and exhibit excellent long-term stability. This development also opens the door to the use of similar materials in low-bandgap solar cells, with potential for tandem or indoor photovoltaic applications. Future work will focus on enhancing signal-to-noise ratios, reducing dark current, and exploring self-powered architectures to further improve performance and broaden applicability.

Data availability

Data for this article is available from the authors upon reasonable request.

Author contributions

Conceptualization of the work was done by D. Zugasti-Fernández, P. Román-Román and D. Solis-Ibarra. Synthesis and characterization of the materials was carried by D. Zugasti-Fernández, P. Román-Román and M. Gutierrez-Avila. V. Jancik measured, solved and refined the single crystal X-ray data. Device fabrication and testing was done by D. Zugasti-Fernández, M. Gutierrez-Avila, J. Hernández-Cordero and N. Hernández-Como. The entire work was supervised by D. Solis-Ibarra and the manuscript was written by D. Zugasti-Fernández, A. P. Gomora-Figueroa and D. Solis-Ibarra with feedback from all other co-authors.

Conflicts of interest

There are no conflicts to declare.

Acknowledgements

This work was financially supported by the Research and Technological Innovation Project Support Program (PAPIIT) under project numbers IN109524 and IT100421. We would like to express our sincere gratitude to Dr M. Hernández-Rodríguez and Dr C. Ortiz-Cervantes from the Institute of Chemistry UNAM, for their invaluable advice and support throughout the development of this work. Similarly, we thank M. in Sc. A. Tejeda-Cruz, for her guidance and assistance in obtaining X-ray diffractograms, and E. Reyes-Morales for her help with Thermogravimetric Analysis (TGA) and Differential Scanning Calorimetry (DSC). Our appreciation extends to M. Canseco and G. Cedillo for their technical expertise in IR, NMR, and UV-vis analysis. We are also grateful to M. in C. A. K. Bobadilla-Valencia for her support through the Department of Condensed Matter and Cryogenics, all of them from the Materials Research Institute (IIM). The assistance of A. Pompa and O. Luna and C. Gónzalez are also acknowledge. N. Hernandez-Como would like to thank CNMN-IPN for the access to the cleanroom. Finally, we would like to express our heartfelt gratitude to Dr C. Pareja-Rivera, M. in Sc. V. López-Cervantes and Dr Y. Amador-Sánchez, for their unwavering support, insightful discussions, and encouragement throughout this project.

References

1 M. A. Green, *Nat. Photonics*, 2008, **92**, 1305–1310, DOI: 10.1038/nphoton.2014.134.
2 S. A. Veldhuis, P. P. Boix, N. Yantara, M. Li, T. C. Sum, N. Mathews and S. G. Mhaisalkar, *Adv. Mater.*, 2016, **28**, 201600669, DOI: 10.1002/adma.201600669.
3 A. Kojima, K. Teshima, Y. Shirai and T. Miyasaka, *J. Am. Chem. Soc.*, 2009, **131**, 6050–6051, DOI: 10.1021/ja809598r.
4 H. Wang, Y. Sun, J. Chen, F. Wang, R. Han, C. Zhang, J. Kong, L. Li and J. Yang, *Nanomaterials*, 2022, **12**, 4390, DOI: 10.3390/nano12244390.
5 C. Bao, J. Yang, S. Bai, W. Xu, Z. Yan, Q. Xu, J. Liu, W. Zhang and F. Gao, *Adv. Mater.*, 2018, **30**, 1803422, DOI: 10.1002/adma.201803422.
6 Y. H. Lee, W. Lee, G. S. Lee, J. Y. Park, B. Yuan, Y. Won, J. Mun, H. Yang, S. Baek, H. Lee, J. H. Oh, T. J. Pennycook, G. Kim, J. Mei and L. Dou, *Adv. Mater.*, 2025, **37**, 2417761, DOI: 10.1002/adma.202417761.
7 J. Li, J. Wang, J. Ma, H. Shen, L. Li, X. Duan and D. Li, *Nat. Commun.*, 2019, **10**, 806, DOI: 10.1038/s41467-019-08768-z.
8 T. Huang, Z. Zhu, C. Zhao, W. Kong, X. Chen, R. Li, Z. Yu, Z. Shi, D. Li, B. Yang and W. Yu, *J. Mater. Chem. A*, 2022, **10**, 21044–21052, DOI: 10.1039/D2TA04288F.
9 K. Dey, B. Roose and S. D. Stranks, *Adv. Mater.*, 2021, **33**, 2102300, DOI: 10.1002/adma.202102300.
10 H. Liu, L. Zhu, H. Zhang, X. He, F. Yan, K. S. Wong and W. C. H. Choy, *ACS Energy Lett.*, 2023, **8**, 577–589, DOI: 10.1021/acsenergylett.2c02055.
11 C. Ortiz-Cervantes, P. I. Román-Román, J. Vazquez-Chavez, M. Hernández-Rodríguez and D. Solis-Ibarra, *Angew. Chem.*, 2018, **130**, 14078–14082, DOI: 10.1002/ange.201809028.
12 P. I. Román-Román, C. Ortiz-Cervantes, J. I. Vasquez-Matias, J. Vazquez-Chavez, M. Hernández-Rodríguez and D. Solis-Ibarra, *ChemSusChem*, 2023, **16**, 202201505, DOI: 10.1002/cssc.202201505.
13 Z. Yang, Y. Deng, X. Zhang, S. Wang, H. Chen, S. Yang, J. Khurgin, N. X. Fang, X. Zhang and R. Ma, *Adv. Mater.*, 2018, **30**, 201704333, DOI: 10.1002/adma.201704333.
14 W. Gao, X. Liu, H. Jin, W. Li, X. Wang, R. Huang, G. Xing, H. Dong, Y. Zhou, Z. Wu and C. Ran, *ACS Energy Lett.*, 2024, **9**, 5045–5055, DOI: 10.1021/acsenergylett.4c01596.
15 Y. Ren, *Adv. Mater. Res.*, 2012, **466–467**, 102–105, DOI: 10.4028/www.scientific.net/AMR.466-467.102.
16 D. Marongiu, M. Saba, F. Quochi, A. Mura and G. Bongiovanni, *J. Mater. Chem. C*, 2019, **7**, 12006–12018, DOI: 10.1039/c9tc04292j.
17 Y. Yu, Y. Zhang, X. Song, H. Zhang, M. Cao, Y. Che, H. Dai, J. Yang, H. Zhang and J. Yao, *Adv. Opt. Mater.*, 2017, **5**, 201700565, DOI: 10.1002/adom.201700565.
18 W. Deng, L. Huang, X. Xu, X. Zhang, X. Jin, S.-T. Lee and J. Jie, *Nano Lett.*, 2017, **17**, 2482–2489, DOI: 10.1021/acs.nanolett.7b00166.
19 G. Konstantatos, M. Badioli, L. Gaudreau, J. Osmond, M. Bernechea, F. P. G. De Arquer, F. Gatti and F. H. L. Koppens, *Nat. Nanotechnol.*, 2012, **7**, 363–368, DOI: 10.1038/nnano.2012.60.
20 Y. Dong, J. Xu, G. Wang, H. Ni, K. Pei, J. Chen, F. Gao, B. Li and Z. Niu, *Electron. Lett.*, 2015, **51**, 1355–1357, DOI: 10.1049/el.2015.1041.
21 F. Li, Y. Chen, C. Ma, U. Buttner, K. Leo and T. Wu, *Adv. Electron. Mater.*, 2017, **3**, 1600430, DOI: 10.1002/aelm.201600430.
22 G. Li, Y. Wang, L. Huang and W. Sun, *ACS Appl. Electron. Mater.*, 2022, **4**, 1485–1505, DOI: 10.1021/acsaelm.1c01349.
23 D. Moses, M. Sinclair, S. Phillips and A. J. Heeger, *Synth. Met.*, 1989, **28**, D675–D681, DOI: 10.1016/0379-6779(89)90760-1.